Materials Transactions, Vol. 61, No. 10 (2020) pp. 2025 to 2029

The Critical Point of Average Grain Size in Phonon Thermal Conductivity of Fine-Grained Undoped Lead Telluride

Mongkol Bumrungpon[1,*1], Issei Morioka[1,*1], Ryusuke Yasufuku[1,*1], Toshiharu Hirai[1,*1], Kenichi Hanasaku[1,*1], Kenji Hirota[1,*1], Katsuhiro Takagi[1,*1] and Kazuhiro Hasezaki[2,*2]

[1]*Graduate School of Advanced Technology and Sciences, Tokushima University, Tokushima 770-8506, Japan*
[2]*Department of Mechanical Science, Graduate School of Technology, Industrial and Social Sciences, Tokushima University, Tokushima 770-8506, Japan*

Undoped PbTe was melted at 1123 K, ball milled (BM) at rotation speeds from 90 to 180 rpm and hot pressed (HP) at 147 MPa and 650 K. Milling at 120 rpm produced the minimum phonon thermal conductivity of 1.29 $W m^{-1} K^{-1}$ and average grain size of 0.80 μm. Phonon thermal conductivity was constant from coarse grain size to fine grain size of 1 μm and decreased suddenly at 0.80 μm. This tendency of phonon thermal conductivity corresponded to theoretical calculations with grain boundary scattering. However, the observed critical point of 1 μm was much larger than the calculated value of 0.03 μm. There was a significant inverse relationship between phonon thermal conductivity and FWHM of X-ray diffraction peaks. The low phonon thermal conductivity was associated with not only grain boundary scattering but high internal strain. [doi:10.2320/matertrans.MT-M2020069]

(Received February 25, 2020; Accepted July 28, 2020; Published September 4, 2020)

Keywords: *eco-materials, thermoelectric materials, powder metallurgy, lead telluride, microstructure*

1. Introduction

Thermoelectricity is a niche research area in which various heat sources can be used to generate electricity. Thermoelectric materials are the cornerstone of commercial thermoelectric generation and many advances have been made in fabricating materials with improved thermoelectric performances.[1–6] Lead telluride (PbTe) thermoelectric generators have been used in various ways, such as powering spacecraft[7] and recovering waste heat from engine exhausts.[8] Thermoelectric performance of materials is evaluated by the dimensionless figure of merit ZT:

$$ZT = \alpha^2 \sigma \kappa^{-1} T \quad (1)$$

where α, σ, κ, and T are Seebeck coefficient ($V K^{-1}$), electrical conductivity ($S m^{-1}$), thermal conductivity ($W m^{-1} K^{-1}$), and absolute temperature (K).

$$\kappa = \kappa_{phonon} + \kappa_{carrier} = \kappa_{phonon} + L\sigma T \quad (2)$$

Carrier component $\kappa_{carrier}$ is given by the Wiedemann–Franz law, where κ_{phonon} is phonon component and L is Lorenz number. The Lorenz number of metals is given by:[9]

$$L = (\pi k_B)^2 (3e^2)^{-1} = 2.45 \times 10^{-8}\ W S^{-1} K^{-2} \quad (3)$$

Various methods have been applied to improve ZT in thermoelectric material, with ZT in the range of 1.4–2.2 at 750–915 K.[10–13] Ideally, thermoelectric materials have high electrical conductivity, high Seebeck coefficients and low thermal conductivity.[14] One strategy for improving ZT is optimizing electronic term $\alpha^2 \sigma \kappa_{carrier}^{-1}$, that is governed by local electronic structure (i.e. density of states, group velocity and relaxation time) near Fermi level, E_f. Another strategy for improving ZT is lowering phonon thermal conductivity κ_{phonon} by providing phonon-scattering centers, e.g., by introducing mass contrast and nanostructures in bulk materials.[15,16]

PbTe performs well in intermediate temperature range 450–850 K and has good chemical and thermal stabilities.[17,18] PbTe melts at 1197 K and crystallizes in NaCl crystal structure (halite, cF8), with Pb atoms occupying cationic sites and Te forming an anionic lattice (space group Fm3m, No. 225), and room-temperature lattice constant 6.462 Å (12.22 bohr). PbTe is a semiconductor with narrow band gap ($E_g \approx 0.25$ eV at 0 K and 0.32 eV at 300 K) and shows either n-type or p-type conductivity depending on deviation from stoichiometry. PbTe has a large exciton Bohr radius of approximately 46 nm, producing charge carrier confinement in relatively large nanostructures.[19] PbTe alloys are promising thermoelectric materials with low thermal conductivity and high-power factors. Theoretical calculation with grain boundary scattering shows that the κ_{phonon} of PbTe bulk materials is constant from coarse grain size to average size of 1 μm and suddenly decreases at 0.01–0.03 μm.[20–22] Ball milling (BM) is effective in preparing homogeneous compounds[23] that allows alloys to form in the solid state via repeated impact during planetary ball milling. Inhomogeneous internal strain creates phonon scattering centers.[24] Ball milling produced internal strain that control lattice thermal conductivity. Lattice softening may affect thermal conductivity beyond grain boundary.[24]

It is known that thermal conductivity of bismuth antimony telluride (BiSbTe) bulk materials changes as milling speed affects grain size.[25] Sufficient planetary ball milling can produce PbTe powder with an average grain size of approximately 0.13 μm.[26,27] However, there is a lack of empirical study of the relationship between thermal conductivity and grain size in PbTe. The present study has focused on undoped bulk PbTe prepared with planetary ball milling. The effects of rotation speed on thermal conductivity were investigated in terms of the relationship between average grain size and phonon thermal conductivity.

*[1]Graduate Student, Tokushima University
*[2]Corresponding author, E-mail: hasezaki@tokushima-u.ac.jp

2. Materials and Methods

Undoped PbTe samples were prepared by melting, planetary ball milling (BM) and hot pressing (HP). Raw materials, Pb (99.998%, 3–5 mm grain size) and Te (99.9999%, 2 mm grain size) were purchased from the Koujundo Chemical Laboratory Co., Ltd. PbTe ingots were melted in evacuated carbon-coated quartz ampoules (10 mm diameter, 120 mm length, columnar cone bottom) that were heated to 1123 K for 3 h under 0.1 Pa, in an electric furnace and quenched with water. The PbTe ingots were placed in a stainless-steel vessel (Fe–Ni–Cr) with Si_3N_4 balls of diameter 25 mm and weight ratio of milling balls to ingots more than 20:1. BM was performed using a Fritsch P-5 planetary ball mill at a rotation speed of 90–180 rpm for 30 h. The stainless-steel vessel was sealed in a glove box under an Ar atmosphere to prevent powder oxidation during milling. Milled powders were passed through a 150 μm diameter sieve to separate unmilled material in a glove box under Ar atmosphere.

Unmilled PbTe ingots and milled powders were then compacted by HP at 650 K under uniaxial pressure of 147 MPa in an Ar atmosphere to prepare for Melting-HP and BM-HP samples, respectively. Hot-pressed compacts (8–10 mm thick, 10 mm diameter) were cut into disks (1 mm thick, 10 mm diameter) to evaluate Seebeck coefficients, electrical conductivity, and thermal conductivity. Determined by Archimedes' method, relative density accuracy was better than ±0.2%.

Structures were investigated by X-ray diffraction (XRD; Rigaku SmartLab, Cu Kα radiation), scanning electron microscopy (SEM; JEOL, JSM-6510A), and focused ion beam (FIB; JEOL, JEM-9320) system. XRD scans (0.1° step size, 0.5 s step time) were conducted for phase identification and internal strain by full width at half maximum (FWHM). Microstructures and grain sizes of the cross-sections were determined by FIB-SEM, SEM. PbTe sintered disk surfaces were polished and chemically etched. Average grain sizes were measured by the linear intercept technique for two-phase polycrystalline.[28)]

Elemental analysis was carried out on PbTe samples by Inductively Coupled Plasma Optical Emission Spectroscopy (ICP-OES), (SII Nano Technology Inc., SPS 3500 Series) to determine contamination after hot-pressing. PbTe samples were crushed into powder to obtain representative samples. PbTe powders (0.2 g) were precisely weighed on a balance and dissolved in a mixture of 30 ml hydrochloric acid (HCl) and 10 ml nitric acid (HNO_3). Once dissolved, the resulting solution was diluted in a volumetric flask with 15 ml de-ionized water. To determine elements in a sample, there was calibration with synthetic standard solutions using Iron (Fe 1000), Chromium (Cr 1000) and Nickel (Ni 1000) standard solutions from FUJIFILM Wako Pure Chemical Co., Ltd. Standard solution was used to determine composition of the original PbTe samples using SPS 3500 Series (ICP-OES).

Seebeck coefficient, electrical conductivity and thermal conductivity were measured at room temperature. Electrical conductivity was measured by a four-point probe (tungsten carbide, 1.0 mm diameter) with a delta-mode electrical resistance system based on a 2182A/6220 instrument (Keithley Instruments, Inc). Measurements were confirmed by ohmic contact to have accuracy better than ±1%. Seebeck coefficient was determined using a constructed thermal contact method. Standard BiTe thermoelectric material (SRM 3451) was used as a reference sample to confirm that accuracy was better than ±2% at room temperature. Thermal conductivity was measured using a constructed static comparison method system. Quartz ($\kappa = 1.411\ W\,m^{-1}\,K^{-1}$) was used as a reference sample and the accuracy was better than ±1%.

3. Results and Discussion

All PbTe samples were *p*-type semiconductors according to measurement of Seebeck coefficient. Table 1 shows absolute and relative densities of Melting–HP and BM-HP samples measured by Archimedes' method.[18)] All samples had relative density of close to 99%. The density did not depend on rotation speed. Thermoelectric properties of sintered materials generally depend on density or porosity. High porosity changes electrical and thermal conductivity. All samples in this study were compact enough to resist the changes.

Figure 1 shows XRD patterns in the 2θ range of 20°–90° for Melting–HP and BM–HP samples. PbTe main indexes are added to the patterns.[18)] XRD pattern peaks indicated a single-phase PbTe crystal structure and there was no peak observed from other materials.

Figure 2 shows full width at half maximum (FWHM) fixed on (200) peaks as a function of milling rotation speed for

Table 1 Milling rotation speed and density of Melting–HP and BM–HP samples.

Milling rotation speed/ rpm	Absolute density ρ/ 10^{-3} kg m^{-3}, relative density (%)
Melting-HP	8.24, 99.8
90	8.21, 99.4
110	8.21, 99.4
120	8.22, 99.5
150	8.23, 99.6
180	8.20, 99.3

Theoretical density 8.26×10^{-3} kg m^{-3} [18)].

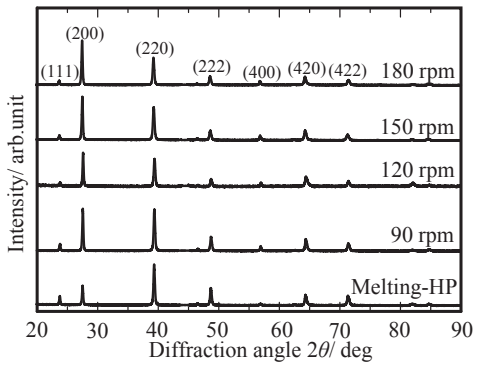

Fig. 1 XRD patterns of PbTe Melting–HP and BM–HP samples milled at rotation speeds from 90 to 180 rpm.[18)]

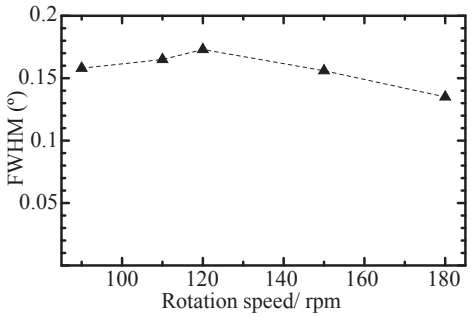

Fig. 2 Full width at half maximum (FWHM) at (200) peaks as a function of milling rotation speed for PbTe samples prepared by BM–HP.

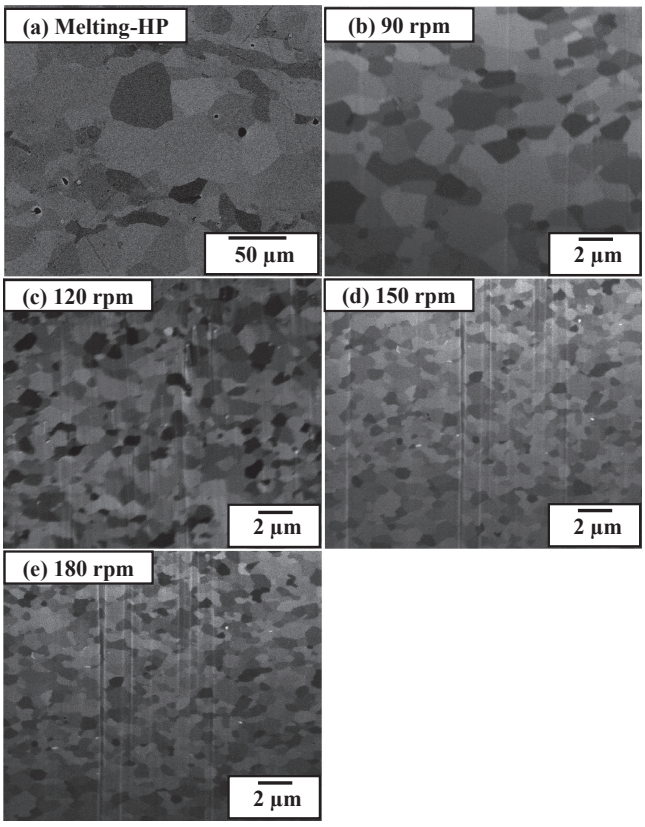

Fig. 3 FIB-SEM micrographs of (a) Melting-HP and BM–HP samples milled at (b) 90 rpm, (c) 120 rpm, (d) 150 rpm and (e) 180 rpm.

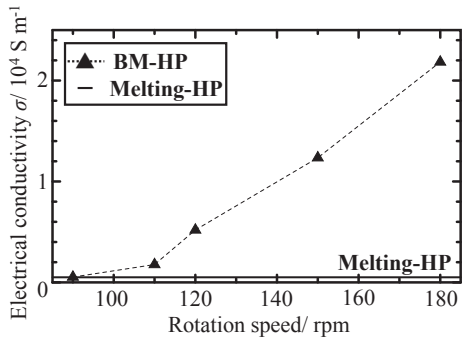

Fig. 4 Electrical conductivity σ at room temperature of Melting-HP and BM-HP as a function of milling rotation speed.

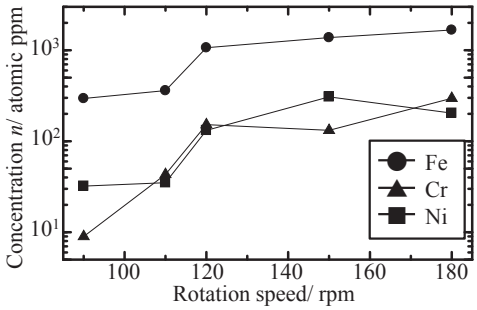

Fig. 5 Concentration of Fe, Cr and Ni elements as a function of milling rotation speed for PbTe samples prepared by BM-HP.

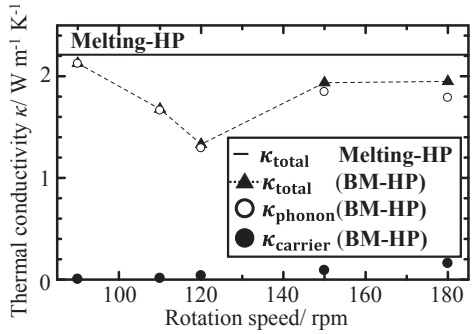

Fig. 6 Total thermal conductivity (κ_{total}), phonon (κ_{phonon}) and carrier ($\kappa_{carrier}$) components at room temperature of Melting-HP and BM-HP as a function of milling rotation speed.

BM-HP samples. The sample milled at 120 rpm depicted the highest FWHM. FWHM is generally proportional to the internal strain. In this study, the sample milled at 120 rpm included the highest internal strain.

Figure 3 shows FIB-SEM micrographs of Melting-HP and BM–HP samples milled at 90, 120, 150 and 180 rpm. All samples had dense and fine grain structures. Measured by the linear intercept technique,[28] Melting-HP sample had average grain size of 22.62 μm. For BM-HP samples, the average grain size decreased with increasing rotation speed: 1.15 μm at 90 rpm, 0.80 μm at 120 rpm, 0.72 μm at 150 rpm and 0.66 μm at 180 rpm.

Figure 4 shows electrical conductivity σ at room temperature of Melting-HP and BM-HP samples as a function of milling rotation speed. Electrical conductivity in Melting–HP sample was similar to that in BM-HP sample milled at 90 rpm. Electrical conductivity of BM-HP samples increased with rotation speed, although no dopant was added.

Figure 5 shows concentration of Fe, Cr, and Ni elements in BM-HP samples determined by ICP-OES. The concentration of impurities increased with rotation speed. Results in Fig. 4 and Fig. 5 are consistent with the relationship between carrier concentration and electrical conductivity.[2] Increase in electrical conductivity was likely to be due to contamination from the stainless-steel milling vessel. Iron (Fe), chromium (Cr) and nickel (Ni) contaminants are estimated to act as *p*-type dopants.

Figure 6 shows total thermal conductivity (κ_{total}), phonon component (κ_{phonon}) and carrier component ($\kappa_{carrier}$) at room temperature of Melting-HP and BM-HP samples as a function of milling rotation speed. κ_{phonon} and $\kappa_{carrier}$ values were estimated from eqs. (2) and (3) (see Introduction). The κ_{phonon} values for PbTe samples prepared by Melting–HP and

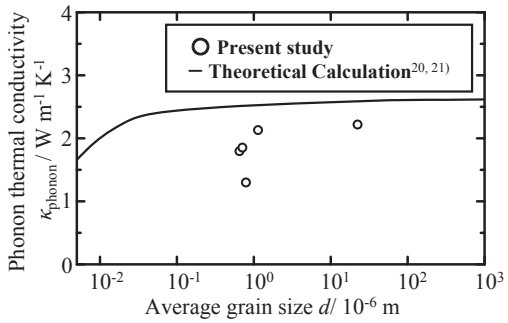

Fig. 7 Relationship between average grain size and phonon thermal conductivity κ_{phonon} at room temperature of Melting-HP and BM-HP. The solid line is the calculated phonon thermal conductivity with grain boundary scattering at 400 K.[20,21]

BM–HP at a rotation speed of 90 rpm were almost same just like electrical conductivity. BM-HP sample at 120 rpm had the minimum κ_{phonon} value of 1.29 W m^{-1} K^{-1} at an average grain size 0.80 µm. The κ_{phonon} in PbTe decreased from 90 rpm to 120 rpm, increased from 120 rpm to 150 rpm and remained relatively constant from 150 rpm to 180 rpm. There was a significant inverse relationship between κ_{phonon} and FWHM (see Fig. 2).

Figure 7 shows the relationship between average grain size and κ_{phonon} at room temperature of Melting-HP and BM-HP for PbTe samples. The calculated κ_{phonon} with grain boundary scattering is constant from coarse grain size to average grain size of 0.1 µm. The critical point of average grain size in κ_{phonon} is approximately 0.03 µm at 400 K.[20,21] The present study showed that the κ_{phonon} was constant at a rotation speed up to 110 rpm and suddenly decreased at 120 rpm. Such a behavior corresponded to the theoretical calculation.[20,21] However, the observed critical point of around 1 µm was much larger than the calculated value of 0.03 µm. High rotation speeds are easy to induce high internal strain in small grains. The internal strain such as dislocations and lattice defects changed phonon frequencies within the material.[24] Internal strain was confirmed to change the critical point from 0.03 µm to 1 µm in PbTe samples prepared by BM–HP.

From these results, the minimum κ_{phonon} was achieved at 120 rpm in PbTe, which led to the maximum internal strain. The rotation speed was a fundamental process parameter to control phonon thermal conductivity.

4. Conclusions

The present study was carried out to investigate the phonon thermal conductivity of undoped PbTe samples, which were prepared by Melting–HP and BM-HP at various rotational speeds using planetary ball milling. The results can be summarized as follows;

(1) XRD patterns indicated that planetary ball milling produced a single-phase PbTe crystal structure. The obtained PbTe samples were dense and the relative densities were higher than 99%.

(2) Average grain sizes of PbTe Melting-HP and BM-HP samples milled at 90, 120, 150 and 180 rpm were 22.62, 1.15, 0.80, 0.72, and 0.66 µm, respectively. They decreased with increasing rotation speed. Thermal conductivity was lowest when the rotation speed reached 120 rpm.

(3) Phonon thermal conductivity was constant from coarse grain size to fine grain size of 1 µm and decreased suddenly at 0.80 µm (120 rpm). This tendency of phonon thermal conductivity corresponded to theoretical calculations with grain boundary scattering. However, the observed critical point of 1 µm was much larger than the calculated value of 0.03 µm.

(4) There was a significant inverse relationship between phonon thermal conductivity and FWHM of X-ray diffraction peaks. The low phonon thermal conductivity of PbTe was associated with not only grain boundary scattering but high internal strain.

Acknowledgements

The authors acknowledge Emeritus Prof. Yasutoshi Noda for valuable discussion. This work was supported by the Takahashi Industrial and Economic Research Foundation.

REFERENCES

1) M.G. Kanatzidis, T. Hogan and S. Mahanti: *Chemistry, Physics, and Materials Science of Thermoelectric Materials: Beyond Bismuth Telluride*, (Springer Science & Business Media, New York, 2012) p. 35.
2) D.M. Rowe: *Thermoelectrics Handbook: Macro to Nano*, (CRC press, Taylor & Francis Group, Boca Raton, Florida, 2006) Ch. 1.
3) G.J. Snyder and E.S. Toberer: *Materials For Sustainable Energy*, (A Collection of Peer-Reviewed Research and Review Articles from Nature Publishing Group, World Scientific, UK, 2011) pp. 101–110.
4) H.J. Goldsmid: *Introduction to Thermoelectricity*, (Springer, Heidelberg Dordrecht, London, 2016) pp. 1–7.
5) C.B. Vining: Nat. Mater. **8** (2009) 83–85.
6) Y. Shinohara: Materials Today: Proceedings **4** (2017) 12333–12342.
7) C. Wood: Rep. Prog. Phys. **51** (1988) 459.
8) D. Champier: Energy Convers. Manage. **140** (2017) 167–181.
9) T.M. Tritt: *Thermal Conductivity: Theory, Properties, and Applications*, (Kluwer Academic/Plenum Publisher, New York, 2004) pp. 1–17.
10) K. Biswas, J. He, I.D. Blum, C.I. Wu, T.P. Hogan, D.N. Seidman, V.P. Dravid and M.G. Kanatzidis: Nature **489** (2012) 414–418.
11) A.D. LaLonde, Y. Pei and G.J. Snyder: Energy Environ. Sci. **4** (2011) 2090–2096.
12) Y. Pei, A. LaLonde, S. Iwanaga and G.J. Snyder: Energy Environ. Sci. **4** (2011) 2085–2089.
13) C. Long, X. Hou, Y. Gelbstein, J. Zhang, B. Ren and Z. Wang: 25th Int. Conf. on Thermoelectrics, Vienna, (2006) pp. 382–385.
14) G. Chen, M.S. Dresselhaus, G. Dresselhaus, J.P. Fleurial and T. Caillat: Int. Mater. Rev. **48** (2003) 45–66.
15) Y. Takagiwa, Y. Pei, G. Pomrehn and G.J. Snyder: Appl. Phys. Lett. **101** (2012) 092102–092103.
16) Y. Takagiwa, Y. Pei, G. Pomrehn and G. Jeffrey Snyder: APL Mater. **1** (2013) 011101–011105.
17) D.R. Lide: *CRC Handbook of Chemistry and Physics: A Ready-Reference Book of Chemical and Physical Data*, (CRC press, Taylor & Francis Group, Boca Raton, Florida, 1995) pp. 4–65.
18) E. Rogacheva, I. Krivulkin, V. Popov and T. Lobkovskaya: Phys. Status Solidi A **148** (1995) K65–K67.
19) A. Jacquot, B. Lenoir, M. Boffoue and A. Dauscher: Appl. Phys., A Mater. Sci. Process. **69** (1999) S613–S615.
20) J. Yoshino: *Theory and Application*, ed. by M. Sakata, (Shokabo, Tokyo, 2005) pp. 44–51.
21) J. Yoshino: *Functionally Graded Materials 1996*, (Elsevier, Amsterdam, 1997) pp. 495–500.
22) C.B. Vining, W. Laskow, J.O. Hanson, R.R. Van der Beck and P.D.

Gorsuch: J. Appl. Phys. **69** (1991) 4333–4340.
23) N. Bouad, M.C. Record, J.C. Tedenac and R.M. Marin-Ayral: J. Solid State Chem. **177** (2004) 221–226.
24) R. Hanus, M.T. Agne, A.J. Rettie, Z. Chen, G. Tan, D.Y. Chung, M.G. Kanatzidis, Y. Pei, P.W. Voorhees and G.J. Snyder: Adv. Mater. **31** (2019) 1900108.
25) M. Kitamura, K. Hirota and K. Hasezaki: Mater. Trans. **59** (2018) 1225–1232.
26) N. Bouad, R. Marin-Ayral and J. Tedenac: J. Alloy. Compd. **297** (2000) 312–318.
27) N. Bouad, R.M. Marin-Ayral, G. Nabias and J.C. Tédenac: J. Alloy. Compd. **353** (2003) 184–188.
28) J.C. Wurst and J.A. Nelson: J. Am. Ceram. Soc. **55** (1972) 109.